If the angles θ_{ij} are related by symmetry, *e.g.* as in a kernel, co-kernel or averaged configuration, it may be simpler to use the explicit relations between the angles:

$$C_{3v}(xxx): 2\cos(\theta_{23}+\varepsilon) = 3\cos^2(\theta_{12}+\varepsilon) - 1$$

$$D_{2d}(x): \quad \cos(\theta_{12}+\varepsilon) + 2\cos(\theta_{13}+\varepsilon) = -1$$

$$D_2: \cos(\theta_{12}+\varepsilon) + \cos(\theta_{13}+\varepsilon) + \cos(\theta_{14}+\varepsilon) = -1$$

$$C_{2v}(x): 4\cos^2(\theta_{13}+\varepsilon) = [1+\cos(\theta_{12}+\varepsilon)] \times [1+\cos(\theta_{34}+\varepsilon)]$$

$$C_2(x): [\cos(\theta_{13}+\varepsilon) + \cos(\theta_{14}+\varepsilon)]^2 = [1+\cos(\theta_{12}+\varepsilon)][1+\cos(\theta_{34}+\varepsilon)]$$

$$C_2(xyy): 2[\cos^2(\theta_{13}+\varepsilon) + \cos^2(\theta_{23}+\varepsilon) - 2\cos(\theta_{12}+\varepsilon) \times \cos(\theta_{13}+\varepsilon)\cos(\theta_{23}+\varepsilon)] = \sin^2(\theta_{12}+\varepsilon)[1+\cos(\theta_{34}+\varepsilon)].$$

References

BAUR, W. H. (1970). *Trans. Am. Crystallogr. Assoc.* **6**, 129–155.

BAUR, W. H. (1974). *Acta Cryst.* B**30**, 1195–1215.

BROWN, I. D. & SHANNON, R. D. (1973). *Acta Cryst.* A**29**, 266–282.

CALVO, C. (1969). *Can. J. Chem.* **47**, 3409–3416.

HILDEBRANDT, R. L., HORNER, G. D. & BOUDJOUK, P. (1976). *J. Am. Chem. Soc.* **98**, 7476–7480.

JØRGENSEN, C. K. (1971). *Acc. Chem. Res.* **4**, 307–315.

LAGER, G. A. & GIBBS, G. V. (1973). *Am. Mineral.* **58**, 756–764.

LOUISNATHAN, S. J. & GIBBS, G. V. (1972). *Mater. Res. Bull.* **7**, 1281–1292.

MCDONALD, W. S. & CRUICKSHANK, D. W. J. (1967). *Acta Cryst.* **22**, 37–43.

MCDOWELL, R. S. (1965). *J. Mol Spectrosc.* **17**, 365–367.

MACKAY, A. L. (1974). *Acta Cryst.* A**30**, 440–447.

MURRAY-RUST, P., BÜRGI, H. B. & DUNITZ, J. D. (1975). *J. Am. Chem. Soc.* **97**, 921–922.

WILSON, E. B., DECIUS, J. C. & CROSS, P. C. (1955). *Molecular Vibrations. The Theory of Infrared and Raman Vibrational Spectra.* New York: McGraw-Hill.

Acta Cryst. (1978). B**34**, 1793–1803

Distortions of MX_4 Molecules from T_d Symmetry. II. Analysis of PO_4, SO_4 and $AlCl_4$ Species

BY PETER MURRAY-RUST

Department of Chemistry, University of Stirling, Stirling, Scotland

AND H. B. BÜRGI AND J. D. DUNITZ

Laboratories of Inorganic and Organic Chemistry, Swiss Federal Institute of Technology, Universitätstrasse 16, 8006 *Zürich, Switzerland*

(*Received* 5 *December* 1977; *accepted* 14 *January* 1978)

Deformations of PO_4, SO_4 and $AlCl_4$ fragments observed in crystals are analysed in terms of symmetry coordinates and internal coordinates. Various correlations among individual components of the total deformation are described and used to derive features of the potential-energy hypersurface of tetrahedral MX_4 fragments. Some of the observed correlations for all three systems can be described by a common numerical function based on the Pauling bond-number concept.

1. General background

Many MX_4 molecules that are known or expected to show T_d symmetry as isolated particles deviate from this symmetry in crystal environments. The observed distortions have been related to models of intramolecular bonding (McDonald & Cruickshank, 1967; Bartell, Su & Yow, 1970; Lager & Gibbs, 1973) as well as to the influence of the crystal environment (McGinnety, 1972). The interdependence of bond-length and bond-angle variations has been studied empirically by Baur (1970, 1974) and by Brown & Shannon (1973).

In this paper we adopt a different point of view. Our premise is that any correlation found among independent parameters defining the structure of a given fragment, *e.g.* MX_4, in a variety of environments maps a region of low potential energy on the corresponding

energy hypersurface. As shown previously (Bürgi, 1973; Bürgi, Dunitz & Shefter, 1973, 1974; Muetterties & Guggenberger, 1974; Holmes & Deiters, 1977), this kind of approach can provide information about details of chemical reaction paths. A preliminary account of some results on MX_4 molecules has appeared (Murray-Rust, Bürgi & Dunitz, 1975, hereinafter MBD 1).

In searching for structural correlations we can simply examine the usual internal coordinates (*e.g.* bond lengths, angles) describing the fragments. However, if we choose to regard the fragments in question as distorted versions of symmetrical reference structures, there are advantages in using symmetry coordinates instead.

2. Symmetry coordinates

Any distortion of a non-linear molecule of N atoms from a specified reference geometry can be represented by a $(3N-6)$-dimensional distortion vector $\mathbf{D} = d_i\mathbf{p}_i = [d_i(\text{obs}) - d_i(\text{ref})]\mathbf{p}_i$ which, in general, transforms as a reducible representation of the point group of the reference molecule with structural parameters d_i(ref). Methods for decomposing such a vector into components that transform as irreducible representations, *i.e.* components D_i along symmetry coordinates $\mathbf{S}_i$, are well known and are discussed in detail in the preceding paper (Murray-Rust, Bürgi & Dunitz, 1978; hereinafter MBD 2) for the special case of MX_4 molecules with T_d reference symmetry.

For convenience, these components are listed below:

$$D_1(A_1) = \tfrac{1}{2}(r_1 + r_2 + r_3 + r_4 - 4r_0)$$

$$D_{3a}(T_2) = \tfrac{1}{2}(r_1 + r_2 - r_3 - r_4)$$

$$D_{3b}(T_2) = \tfrac{1}{2}(r_1 - r_2 + r_3 - r_4)$$

$$D_{3c}(T_2) = \tfrac{1}{2}(r_1 - r_2 - r_3 + r_4)$$

$$D_{2a}(E) = \frac{1}{\sqrt{12}}(2\alpha_{12} - \alpha_{13} - \alpha_{14} - \alpha_{23} - \alpha_{24} + 2\alpha_{34})$$

$$D_{2b}(E) = \tfrac{1}{2}(\alpha_{13} - \alpha_{14} - \alpha_{23} + \alpha_{24})$$

$$D_{4a}(T_2) = \frac{1}{\sqrt{2}}(\alpha_{12} - \alpha_{34})$$

$$D_{4b}(T_2) = \frac{1}{\sqrt{2}}(\alpha_{13} - \alpha_{24})$$

$$D_{4c}(T_2) = \frac{1}{\sqrt{2}}(\alpha_{14} - \alpha_{23})$$

$$D_5(A_1) = \frac{1}{\sqrt{6}}(\alpha_{12} + \alpha_{13} + \alpha_{14} + \alpha_{23} + \alpha_{24} + \alpha_{34} - 6\alpha_0)$$

with $r_0 = r$(ref) and $\alpha_0 = 109{\cdot}47°$. The bond lengths transform as $A_1 + T_2$, the bond angles as $E + T_2$, with an additional redundant coordinate (the sum of the angles) transforming as A_1.

3. Analysis of distorted PO_4 fragments in terms of symmetry coordinates

Our analysis of distorted PO_4 fragments is based on Baur's (1974) compilation. For each of the 211 PO_4 fragments listed by Baur, the components of the distortion vector along symmetry coordinates were evaluated. For self-consistency, we label the O atoms (tetrahedral vertices) such that $r_1 \geq r_2 \geq r_3 \geq r_4$; this implies that $D_{3a} \geq D_{3b} \geq D_{3c}$ and that the first two components are positive. However, the above labelling convention for the vertices does not impose any restriction on the components of the angle deformation vectors $\mathbf{D}_2$ and $\mathbf{D}_4$.

The data were searched for possible trends or correlations among the symmetry-coordinate components of the deformation vectors **D**. Fig. 1 shows the distribution of the product $|\mathbf{D}_3|.|\mathbf{D}_4|$ against $\cos\psi = \mathbf{D}_3.\mathbf{D}_4/|\mathbf{D}_3|.|\mathbf{D}_4|$, where ψ is the angle between the vectors $\mathbf{D}_3$ and $\mathbf{D}_4$. It is evident that large products tend to be associated with ψ angles close to 180° ($\cos\psi = -1$). In other words, if both vectors are large, there is a correlation between their directions; the two vectors tend to be antiparallel, so that $-\mathbf{D}_4$ and $\mathbf{D}_3$ tend to lie in corresponding regions of their respective deformation spaces.

Fig. 2 shows the distribution of D_{3a} against D_{4a}. According to our labelling convention, D_{3a} is the largest

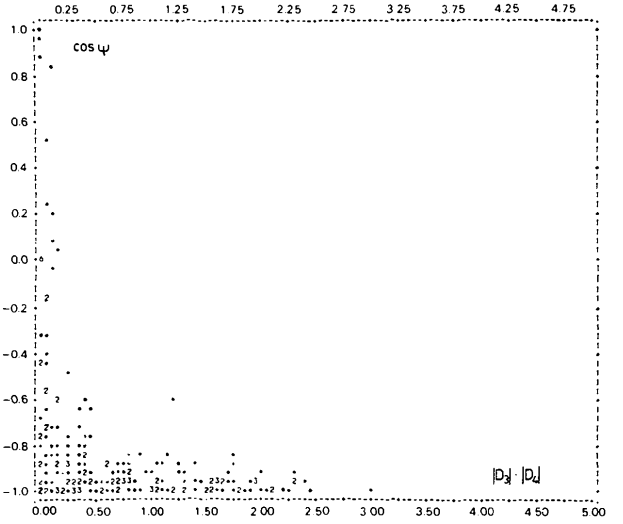

Fig. 1. Distribution of $\cos\psi = \mathbf{D}_3.\mathbf{D}_4/|\mathbf{D}_3|.|\mathbf{D}_4|$ against $|\mathbf{D}_3|.|\mathbf{D}_4|$. The numbers denote frequency of incidence, single incidence being denoted by an asterisk.

component of $\mathbf{D}_3$ in the chosen coordinate system; D_{4a} is not necessarily the largest component of $\mathbf{D}_4$, but, because of the correlation shown in Fig. 1, it will tend to be so. It is seen from Fig. 2 that the correlation between D_{3a} and D_{4a} is essentially linear [D_{3a}(Å) = −0·0091 D_{4a}(°)] and highly significant ($R = -0{\cdot}96$).

Linear regression treats one variable (D_{3a}) as dependent and the other (D_{4a}) as independent. In order to avoid the arbitrariness involved in choosing dependent and independent variables, the principal axes of inertia (eigenvectors) were calculated for a distribution containing the points of Fig. 2 and those generated by inversion across the origin. The larger eigenvector (to be compared with the regression line) is along D_{3a} (Å) = −0·0094 D_{4a} (°).

We can interpret the observed linear interdependence of D_{3a} and D_{4a} as a manifestation of a non-zero cross-term k_{34} in the quadratic approximation to the corresponding part of the potential energy expression

$$2V = k_{33}D_{3a}^2 + k_{44}D_{4a}^2 + 2k_{34}D_{3a}D_{4a}. \qquad (1)$$

The potential constants k_{33} and k_{44} are positive. If k_{34} is also positive, $2V$ is larger in the first quadrant than in the second, and our premise would then imply that distortions along $+\mathbf{S}_{3a}$ should be associated with distortions along $-\mathbf{S}_{4a}$, as actually observed (Fig. 2). We conclude therefore that k_{34} is positive. We can even proceed a little further since, according to our premise, the slope of the eigenvector $D_{3a}/D_{4a} = g \sim -0{\cdot}0094$ Å deg^{-1} can be identified with the direction of minimal energy increase, the major axis of the set of ellipses, V = constant.

By symmetry, D_{3a} and D_{4a} in (1) may be replaced by D_{3b} and D_{4b} or by D_{3c} and D_{4c}, the potential constants being invariant to the choice of axes. It follows that (1) may be rewritten in terms of the actual deformation vectors:

$$2V = k_{33}|\mathbf{D}_3|^2 + k_{44}|\mathbf{D}_4|^2 + 2k_{34}\,\mathbf{D}_3.\mathbf{D}_4 \qquad (1')$$

so that the observed correlation between major components of the vectors must also hold approximately for the vectors themselves.

In contrast to the linear correlation between $D_{3a}(T_2)$ and $D_{4a}(T_2)$ (Fig. 2), the distribution of $D_1(A_1)$ against $|\mathbf{D}_2(E)|$ (Fig. 3) shows that these two quantities are essentially uncorrelated. This distribution is compatible with a potential-energy expression

$$2V = k_{11}D_1^2 + k_{22}|\mathbf{D}_2|^2 \qquad (2)$$

involving only squared terms. Since the two coordinates here transform as different irreducible representations and the potential energy must be invariant to any symmetry transformation, the cross-term $k_{12}D_1(A_1)|\mathbf{D}_2(E)|$ has to disappear, *i.e.* k_{12} has to be identically zero. In the same way, cross-terms between all pairs of coordinates transforming as different irreducible representations must also be zero as long as the quadratic approximation for the potential energy holds.

For large deformations from the T_d reference symmetry, the quadratic approximation cannot be expected to hold. Although there can be no linear correlation between deformation components transforming as different irreducible representations, higher-order correlations are not excluded and indeed are to be

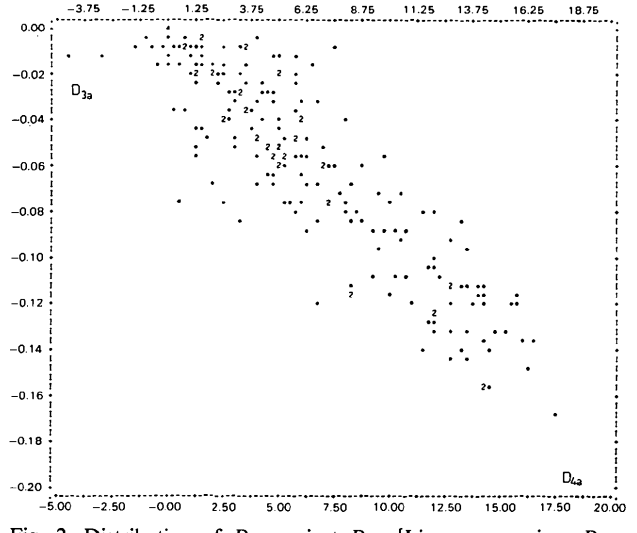

Fig. 2. Distribution of D_{3a} against D_{4a}. [Linear regression: D_{3a} (Å) = −0·0091 D_{4a} (°), correlation: $R = -0{\cdot}96$; the eigenvector belonging to the larger eigenvalue of the distribution D_{3a}, D_{4a} has a slope $D_{3a}/D_{4a} = -0{\cdot}0094$ Å deg^{-1}.]

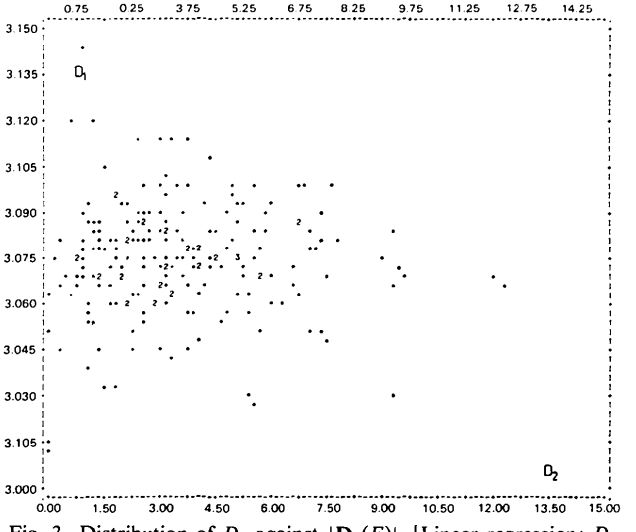

Fig. 3. Distribution of D_1 against $|\mathbf{D}_2(E)|$. [Linear regression: D_1 (Å) = 0·00004 $|\mathbf{D}_2(E)$ (°)| +3·075; correlation $R = 0{\cdot}006$.]

expected in some cases. For example, a large bond-length deformation along $\mathbf{S}_{3a}(T_2)$ would have to be coupled to a deformation along $\mathbf{S}_1(A_1)$ to prevent undue shortening of two of the $M-X$ bonds. From the scatter plot of D_1 against $|\mathbf{D}_3|$ (Fig. 4) it is seen that for small $|\mathbf{D}_3|$ the points scatter about the line $D_1 = 3{\cdot}07$ Å, but, as $|\mathbf{D}_3|$ increases, they tend to lie above this line. In place of a linear correlation we have an approximately quadratic one, $D_1 \sim 3{\cdot}07$ Å $+ h|\mathbf{D}_3|^2$ with $h \sim 1{\cdot}21$ Å^{-1}. A quadratic correlation of this kind would correspond to a cubic cross-term $k_{133}D_1|\mathbf{D}_3|^2$ in the appropriate part of the potential energy expression. The distribution of $|\mathbf{D}_2(E)|$ against $|\mathbf{D}_4(T_2)|$ is more difficult to interpret, but it shows that for nearly 90% of the MX_4 fragments $|\mathbf{D}_4(T_2)| > |\mathbf{D}_2(E)|$.

Similarly, for large distortions the potential energy in each of the two T_2 subspaces can no longer be expected to be spherically symmetrical, although it must still be totally symmetric with respect to the symmetry operations of T_d. Thus, for example, although equal and opposite deformations along $\mathbf{S}_{3a}$ or $\mathbf{S}_{4a}$ have the same energy since they correspond to isometric structures, equal and opposite deformations along $\mathbf{S}_{3a'}$ or $\mathbf{S}_{4a'}$ correspond to non-isometric structures with different energies [see MBD 2 for definitions of primed coordinates and recall that a distortion along $+\mathbf{S}_{3a'}$ corresponds to a C_{3v} distortion with the unique bond stretched (r_1), whereas distortion along $-\mathbf{S}_{3d''}$ corresponds to a C_{3v} distortion with the unique bond contracted (r_4)].

As will be discussed below, most of the MX_4 fragments that show large distortions retain approximate C_{2v} or C_{3v} symmetry. This means that the analysis of large deformations is essentially limited to the description of paths that run along particular directions in the nine-dimensional deformation space. These paths may correspond to channels or tunnels in the potential-energy hypersurface, which would again require the introduction of higher than quadratic terms. It is clear that large deformations imply strong perturbation of the MX_4 fragment by the crystal environment, and we shall return to this point in § 7.

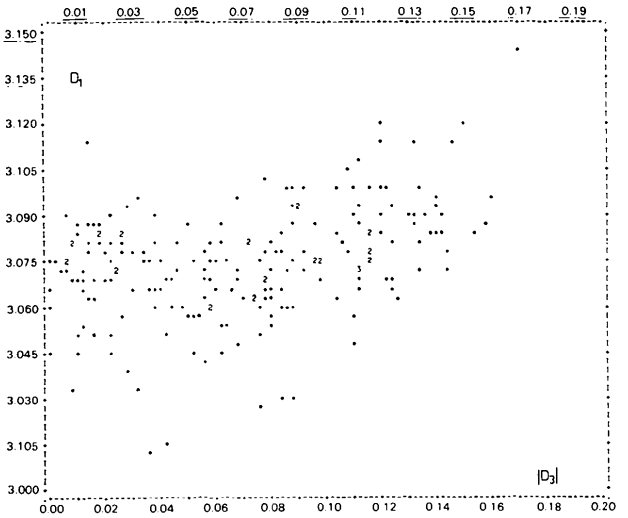

Fig. 4. Distribution of D_1 against $|\mathbf{D}_3|$. [Quadratic regression: D_1 (Å) = 3·067 + 1·21 $|\mathbf{D}_3$ (Å)$|^2$; correlation $R = 0{\cdot}37$.]

The examples discussed in this section suffice to demonstrate that decomposition of the total deformation vector into components along symmetry coordinates can be helpful in the search for correlations among the deformation parameters. The analysis of the deformations observed in different structures can be based on preconceptions about the symmetry properties of the potential-energy hypersurface, and, conversely, any correlations that are found can be interpreted in terms of particular features of this hypersurface.

4. PO_4 fragments with approximate C_{2v} or C_{3v} symmetry

Another advantage of the symmetry-coordinate analysis is that it provides quantitative expression to the concept of approximate symmetry. An example is given in MBD 2. For an MX_4 fragment with *exact* C_{2v} symmetry, the $\mathbf{D}_3$ and $\mathbf{D}_4$ distortion vectors can have non-zero components only along $\mathbf{S}_{3a}$ and $\mathbf{S}_{4a}$, respectively, in our coordinate system. We define a fragment as having *approximate* C_{2v} symmetry if $\mathbf{D}_3$ lies within 20° of $\mathbf{S}_{3a}$. Similarly, we define a fragment as having approximate C_{3v} symmetry if the $\mathbf{D}_3$ vector lies within 20° of $\mathbf{S}_{3a''}$ or $-\mathbf{S}_{3d''}$. We find that approximate C_{2v} or C_{3v} symmetry, as defined above, is displayed by most of the PO_4 fragments showing large distortions. In order to simplify the analysis of MX_4 fragments with approximate symmetry, we consider only the components of the total deformation vector along the symmetry coordinates that preserve the subsymmetry in question. Such a projection of the deformation vector corresponds to an averaging over the internal coordinates that are required to be equal for exact symmetry. There is no problem about averaging the bond distances; however, since the six angles are not independent, straightforward averaging of them may lead to a structure that is unfeasible in three dimensions. Ways of circumventing this difficulty are mentioned in MBD 2 (§ 4.3). For MX_4 fragments retaining C_{2v} symmetry, the deformation space has four dimensions. In symmetry coordinates, these are $\mathbf{S}_1(A_1)$, $\mathbf{S}_{2a}(E)$, $\mathbf{S}_{3a}(T_2)$ and $\mathbf{S}_{4a}(T_2)$; in internals, they are $\mathbf{r}_{(1,2)}$, $\mathbf{r}_{(3,4)}$, $\boldsymbol{\alpha}_{12}$ and $\boldsymbol{\alpha}_{34}$. For MX_4 fragments retaining C_{3v} symmetry, the deformation space has only three dimensions: $\mathbf{S}_1(A_1)$, $\mathbf{S}_{3a''}(T_2)$ and $\mathbf{S}_{4a''}(T_2)$ in symmetry coordinates, and $\mathbf{r}_1$, $\mathbf{r}_{(2,3,4)}$ and $\boldsymbol{\alpha}_{(12,13,14)}$ in internals. In both cases, the remaining angles are dependent variables (see MBD 2 Appendix for the relevant trigonometric relations).

For the C_{2v} case, the transformations between components along internal and symmetry coordinates are:

$$\begin{aligned}
(r_1 + r_2 - 2r_0)/2 = \ & \langle \delta r \rangle_{1,2} = \tfrac{1}{2}(D_1 + D_{3a}) \\
(r_3 + r_4 - 2r_0)/2 = \ & \langle \delta r \rangle_{3,4} = \tfrac{1}{2}(D_1 - D_{3a}) \\
(\alpha_{12} - \alpha_0) = \ & \delta\alpha_{12} = \frac{1}{\sqrt{3}} D_{2a} + \frac{1}{\sqrt{2}} D_{4a} \\
(\alpha_{34} - \alpha_0) = \ & \delta\alpha_{34} = \frac{1}{\sqrt{3}} D_{2a} - \frac{1}{\sqrt{2}} D_{4a}
\end{aligned} \tag{3}$$

assuming $\sum \delta\alpha_{ij} = 0$. The gradual admixture of D_{2a} to D_{4a} is apparent in Fig. 5, which shows the distribution of α_{12} against α_{34} for 91 PO_4 fragments with approximate C_{2v} symmetry. This distribution, which is symmetric about the line $\alpha_{12} = \alpha_{34}$, shows a detectable deviation from the linearity that would hold if D_{2a} were zero everywhere. The slope of the curve at $\alpha_{12} = \alpha_{34} = 109{\cdot}47°$ is fixed by symmetry and equals -1. In order to estimate the curvature, we have chosen to calculate the regression

$$(\alpha_{12} + \alpha_{34})/\sqrt{2} = A + B(\alpha_{12} - \alpha_{34})^2/2.$$

The linear combinations of α's in this expression are respectively symmetric and antisymmetric across the mirror line $\alpha_{12} = \alpha_{34}$. For a regular tetrahedron, $A = 154{\cdot}82°$, and by regression we find $A = 155{\cdot}0\,(3)°$, $B = 0{\cdot}007\,(2)$ deg^{-1}. The observed curvature agrees with that expected from the relation

$$\cos\alpha_{12} + \cos\alpha_{34} = 3\cos\alpha_{12}\cos\alpha_{34} - 1$$

derived from a simple sp^3-hybridization model. It also agrees with the simpler *ad hoc* assumption, $\cos\alpha_{12} + \cos\alpha_{34} = -\frac{2}{3}$.

Similarly, the distribution of $\langle r \rangle_{1,2}$, the mean of r_1 and r_2, against $\langle r \rangle_{3,4}$ shows the admixture of D_1 when the difference between these two quantities becomes large. Fig. 6 contains the distributions of $\langle r \rangle_{i,j}$ against included angle α_{ij} (bottom) and opposite angle α_{kl} (top). It contains all the information needed to construct the correlation curve in the corresponding four-dimensional deformation space. For example, given $\langle r \rangle_{1,2}$, we can determine α_{12} from one plot and α_{34} from the other, whence $\langle r \rangle_{3,4}$ may be read from either plot.

The main trend observed in the distributions shown in Fig. 6 may be expressed in terms of a linear correlation between $\langle \delta r \rangle_{1,2}$ and the included and opposite angles. The slopes of these lines can be derived

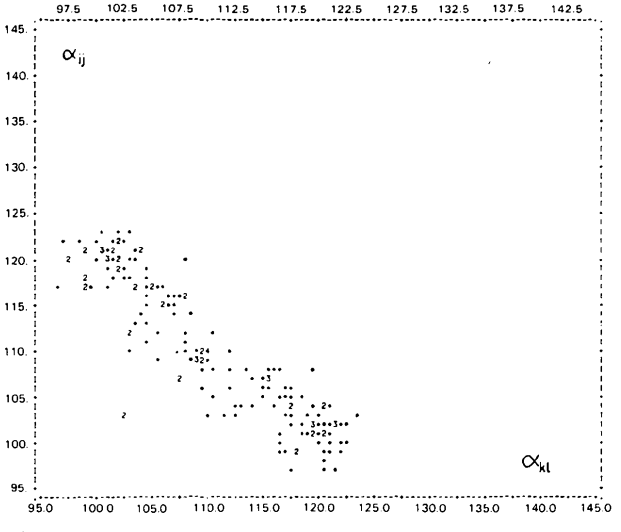

Fig. 5. Distribution of α_{ij} against α_{kl} for 91 PO_4 fragments with approximate C_{2v} symmetry. [Angle against opposite angle; quadratic regression: $(\alpha_{ij} + \alpha_{kl})/\sqrt{2} = 155{\cdot}0 + 0{\cdot}007\ (\alpha_{ij} - \alpha_{kl})^2/2$; angles in degrees; see also text.]

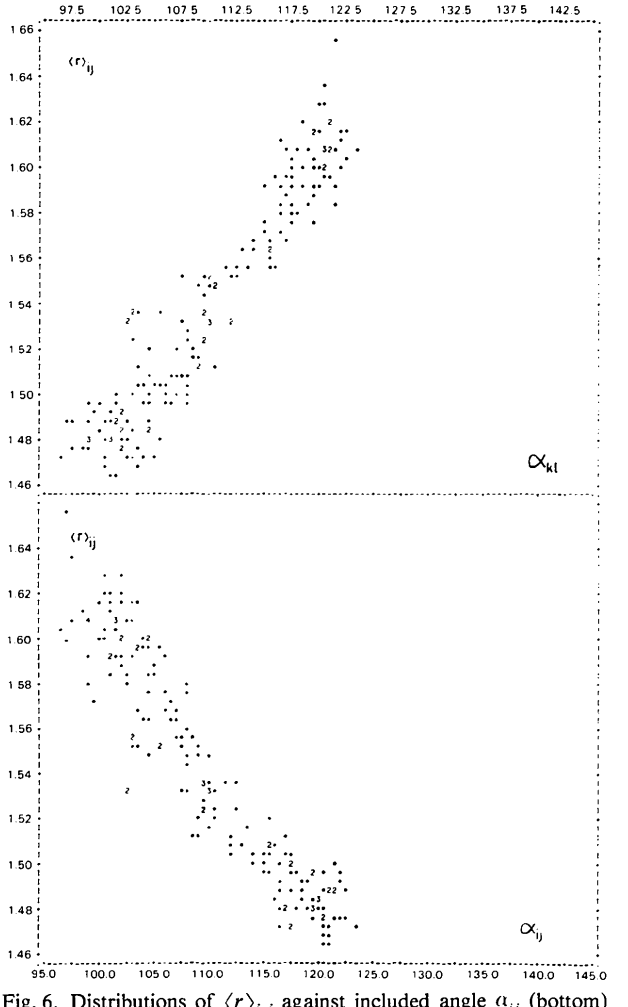

Fig. 6. Distributions of $\langle r \rangle_{i,j}$ against included angle α_{ij} (bottom) and opposite angle α_{kl} (top) for 91 PO_4 fragments with approximate C_{2v} symmetry. [Linear regressions: $\langle r \rangle_{i,j}$ (Å) = $2{\cdot}221 - 0{\cdot}0062\ \alpha_{ij}$ (°), correlation $R = -0{\cdot}94$; $\langle r \rangle_{i,j}$ (Å) = $2{\cdot}221 + 0{\cdot}0062\ \alpha_{kl}$ (°), correlation $R = 0{\cdot}95$.]

from (3) by considering only the T_2 part of the total deformation vector, *i.e.* by assuming $D_1(A_1) = D_{2a}(E) = 0$. Under these conditions

$$D_{3a} = 2\langle\delta r\rangle_{1,2},$$
$$D_{4a} = \sqrt{2}\,\delta\alpha_{12}. \tag{4}$$

We have already found a linear correlation, $D_{3a} = gD_{4a}$, with $g \sim -0{\cdot}0094$ Å deg^{-1}. It follows that

$$\langle\delta r\rangle_{1,2} = \frac{g}{\sqrt{2}}\,\delta\alpha_{12}. \tag{5}$$

The result is general; it holds for any two bonds and the angle between them and is the basis of the correlation found by Baur (1974) between the mean length of a pair of P—O bonds and the included O—P—O angle. There is, of course, an analogous relation between the mean length of a pair of P—O bonds and the opposite O—P—O angle:

$$\langle\delta r\rangle_{1,2} = \frac{-g}{\sqrt{2}}\,\delta\alpha_{34}. \tag{6}$$

The slope obtained from the 91 structures with approximate C_{2v} symmetry (Fig. 6) is 0·0062 Å deg^{-1}, to be compared with the value $g/\sqrt{2} = 0{\cdot}0066$ Å deg^{-1} from the D_{3a}/D_{4a} correlation (Fig. 2) based on the complete data.

For large distortions from T_d symmetry, the linearity of the relations between bond lengths and angles breaks down. Because of the non-quadratic nature of the potential-energy function, the T_2 type deformations should become increasingly mixed with A_1 and E type deformations. The expected deviations from linearity are just discernible in the experimental distributions of Fig. 6.

For the C_{3v} case, the transformations between components along internal and symmetry coordinates are, for the unique bond length, the averaged bond length, and the averaged angle:

$$r_1 - r_0 = \delta r_1 = \tfrac{1}{2}(D_1 + \sqrt{3}D_{3a'})$$
$$\tfrac{1}{3}(r_2 + r_3 + r_4 - 3r_0) = \langle r\rangle_{2,3,4} - r_0 = \delta r_2$$
$$= \frac{1}{2}\left(D_1 - \frac{1}{\sqrt{3}}\,D_{3a'}\right) \tag{7}$$

$$\tfrac{1}{3}(\alpha_{12} + \alpha_{13} + \alpha_{14} - 3\alpha_0) = \langle\alpha\rangle_{12,13,14} - \alpha_0$$
$$= \delta\alpha = \frac{1}{\sqrt{6}}\,D_{4a'}$$

again assuming $\sum \delta\alpha_{ij} = 0$. The distributions shown in Fig. 7 are based on 68 structures with approximate C_{3v} symmetry from Baur's list.

In the linear region close to T_d symmetry, the increase in δr_1 is three times the decrease in δr_2, as expected from (7) when D_1 is negligible. The observed slope $\mathrm{d}(\delta r_1)/\mathrm{d}(\delta\alpha)$ is $-0{\cdot}018$ Å deg^{-1}, to be compared with the value $-3g/\sqrt{2} = -0{\cdot}020$ Å deg^{-1} when g is obtained from the D_{3a}/D_{4a} correlation. For larger distortions the component along $\mathbf{S}_1$ becomes appreciable, and this should produce a positive curvature in the $\delta r_1/\delta\alpha$ and the $\delta r_2/\delta\alpha$ scatter plots. This feature is hardly discernible in the distributions of Fig. 7, but it becomes more evident in the corresponding distributions for SO_4 and $AlCl_4$ fragments to be discussed later.

The separate analyses of PO_4 fragments retaining approximate C_{2v} and C_{3v} symmetry not only serve to delineate tunnels or channels in the potential energy surface but also allow us to test the validity of an assumption implicit in (1′), namely, that the quadratic

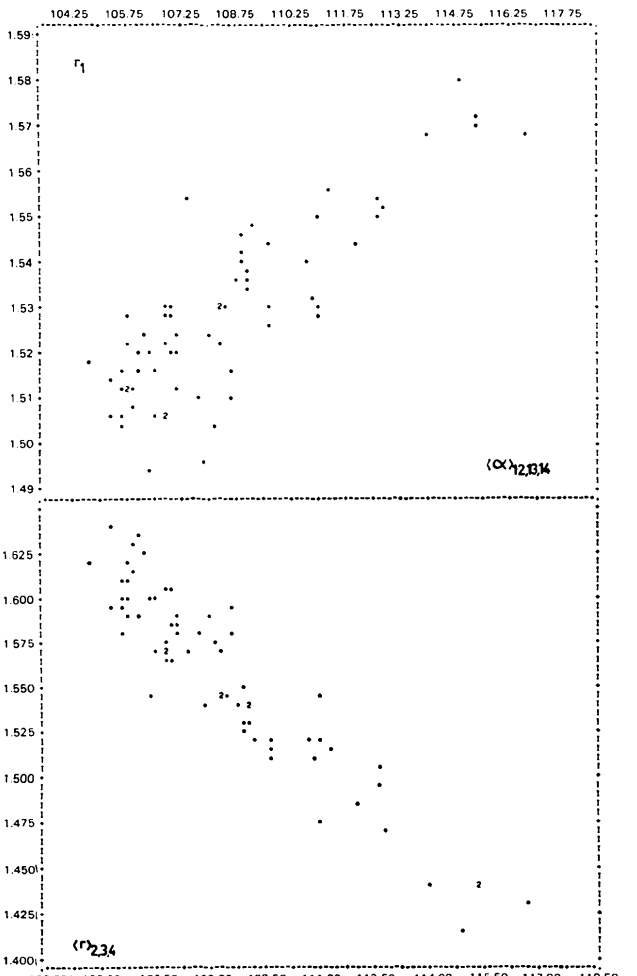

Fig. 7. Distributions of r_1 against $\langle\alpha\rangle_{12,13,14}$ (top) and $\langle r\rangle_{2,3,4}$ against $\langle\alpha\rangle_{12,13,14}$ (bottom). [Linear regressions: r_1 (Å) = 3·490 − 0·0179 $\langle\alpha\rangle_{12,13,14}$ (°), correlation $R = -0{\cdot}93$; $\langle r\rangle_{2,3,4}$ (Å) = 0·903 + 0·0058 $\langle\alpha\rangle_{12,13,14}$ (°), correlation $R = 0{\cdot}84$.]

potential is independent of the individual directions of $\mathbf{D}_3$ and $\mathbf{D}_4$ and depends only on the angle between them. If this assumption were correct, g [and hence $k_{34}/(k_{33}-k_{44})$] would have to be the same for distortion vectors with components D_{3a}, D_{4a} (C_{2v} symmetry) as for vectors with components $D_{3a''}$, $D_{4a''}$ (C_{3v} symmetry). The close agreement of observed slopes $\mathrm{d}(\delta r)/\mathrm{d}(\delta\alpha)$ for PO_4 fragments retaining approximate C_{2v} or C_{3v} symmetry with the slopes derived from g thus confirms the approximate validity of the assumption of a spherically symmetric, quadratic potential for small distortions.

5. SO_4 and $AlCl_4$ fragments

So far our analysis has been limited to PO_4 fragments, and the question arises to what extent our conclusions are also valid for other tetrahedral MX_4 systems. Unfortunately, Baur's exhaustive compilation is restricted to phosphates. For other systems we have confined our analysis to a somewhat arbitrary selection of data culled from the literature. From our point of view the most interesting MX_4 systems are SO_4 and $AlCl_4$ fragments because, for some of these, distortions along the C_{3v} channel ultimately lead to stable products (stable at least in a crystal environment): namely $SO_3 + O^{2-}$ from SO_4^{2-} and $AlCl_3 + Cl^-$ from $AlCl_4^-$. Correlations derived from experimental distributions for these systems could thus serve to delineate reaction pathways for ligand dissociation. With this in mind we have gathered data for 26 SO_4 fragments and for SO_3 (Table 1) as well as for 17 $AlCl_4$ fragments and for $AlCl_3$ (Table 2), all of which show at least approximate C_{3v} symmetry. The data have been selected from various sources: (*a*) SO_3 and $AlCl_3$ from gas-phase electron diffraction investigations, (*b*) SO_4 and $AlCl_4$ fragments from the *BIDICS* 1969–72 bibliography of inorganic crystal structures (Brown, 1969). The selection has been guided by the following criteria: (*c*) Inclusion of fragments if $|\delta r_1| < 0{\cdot}05$ Å (approximate T_d symmetry) *or* $0{\cdot}05 \le |\delta r_1| \le 0{\cdot}15$ Å and differences among r_2, r_3, r_4 smaller than 3σ *or* $|\delta r_1| > 0{\cdot}15$ Å (approximate C_{3v} symmetry). (*d*) Exclusion of structures with disorder or large thermal motion in the MX_4 fragment. (*e*) Exclusion of inaccurate structures [$\sigma(r) > 0{\cdot}02$ Å].

Table 1. *Structural parameters for* SO_4 *fragments with approximate* C_{3v} *symmetry*

Compound	r_1	$\langle r\rangle_{2,3,4}$	$\langle\alpha\rangle_{12,13,14}$	Reference
$K_2S_5O_{16}$	1·403 Å	1·526 Å	112·1°	1
$FeNH_4(SO_4)_2.3H_2O$	1·434	1·478	111·5	2
$Cu[C_3H_{10}N_2]SO_4.H_2O$	1·440	1·477	109·9	3
$Zn[C(NH_2)_3]_2(SO_4)_2$	1·440	1·470	110·4	4
NH_4LiSO_4	1·450	1·468	109·7	5
$Zn(C_6H_{10}N_3O_4)(H_2O)_4(SO_4)_{1/2}$	1·455	1·455	109·0	6
$(C_9H_{13}N)_2.H_2SO_4$	1·455	1·474	110·3	2
$SnSO_4$	1·457	1·497	111·3	7
K_2SO_4	1·459	1·472	109·7	8
$[(NH_3)_4Co(NH_2,OH)Co(NH_3)_4](SO_4)_2.2H_2O$	1·460	1·469	109·2	9
$NaAl(SO_4)_2.12H_2O$	1·461	1·459	110·1	10
$BeSO_4.4H_2O$	1·464	1·464	109·5	11
$(C_5H_6N_5O)_2SO_4.H_2O$	1·466	1·474	109·6	12
$[(NH_3)_4Co(NH_2,OH)Co(NH_3)_4](SO_4)_2.2H_2O$	1·472	1·469	109·1	9
$Cu(NH_4)_2(SO_4)_2.6H_2O$	1·475	1·471	109·2	13
$(H_5O_2)_2SO_4$	1·479	1·479	109·5	14
$(C_9H_{13}N)_2H_2SO_4$	1·480	1·437	108·3	15
	1·490	1·463	109·0	15
$N_2H_6SO_4$	1·491	1·473	108·7	16
$(C_5H_7N_5O)_2SO_4$	1·494	1·461	108·4	17
$[en_2Co(NH_2,SO_4)Coen_2]Br_3$	1·502	1·456	108·9	18
NH_4HSO_4	1·549	1·430	105·5	19
	1·557	1·445	106·0	19
$C_9H_{11}NO_2SO_4.2H_2O$	1·611	1·442	104·6	20
$K_2S_5O_{16}$	1·668	1·450	103·6	1
	1·826	1·419	100·2	1
$SO_3(g)$	∞	1·418	90	21

References: (1) de Vries & Mijlhoff (1969). (2) Palmer, Wong & Lee (1972). (3) Morosin & Howatson (1970). (4) Morimoto & Lingafelter (1970). (5) Dollase (1969). (6) van der Helm & Nicholas (1970). (7) Donaldson & Puxley (1972). (8) McGinnety (1972). (9) Schaeffer & Lighty (1972). (10) Kay & Cromer (1970). (11) Sikka & Chidambaram (1969). (12) Subramanian & Marsh (1971). (13) Brown & Chidambaram (1969). (14) Kjällman & Olovsson (1972). (15) Bergin & Carlström (1971). (16) Jönsson & Hamilton (1970). (17) Prusiner & Sundaralingam (1972). (18) Thewalt (1971). (19) Nelmes (1971). (20) Fries & Sundaralingam (1971). (21) Clark & Beagley (1971).

The appropriate bond lengths and angles were averaged to produce structures with C_{3v} symmetry. Results are given in Tables 1 and 2, which serve as a basis for the distributions shown in Figs. 8 and 9. These distributions show larger deviations from T_d symmetry than the corresponding PO_4 distribution (Fig. 7), but apart from that, all three distributions are very similar. In particular, the observed slopes $d(\delta r_1)/d(\delta\alpha)$ in the linear region close to T_d geometry are practically equal for $AlCl_4$, SO_4 and PO_4, in spite of the differences in mean bond lengths. If the three distributions are given in terms of $\delta r = r - r_0$, *i.e.* if they are referred to a common origin, the sample points appear to be drawn from a single population. The points for planar $AlCl_3$ and SO_3 lie close to the smooth curves shown.

6. Description of correlations by analytical functions

The smooth curves shown in Figs. 8 and 9 are not just correlation curves of arbitrary form drawn to fit the data as well as possible. Rather, they represent an attempt to reproduce the observed general trends in terms of a simple model of chemical bonding based on Pauling's (1947) relation between bond length and bond number;

$$\delta r_i = r_i - R = -c \log n_i \qquad (8)$$

where R is the single-bond length, taken here as r_0.

Table 2. *Structural parameters for* $AlCl_4$ *fragments with approximate* C_{3v} *symmetry*

Compound	r_1	$\langle r\rangle_{2,3,4}$	$\langle\alpha\rangle_{12,13,14}$	Reference
$Se_8(AlCl_4)_2$	2·07 Å	2·143 Å	111·7°	1
$C_6H_6.U.(AlCl_4)_3$	2·07	2·167	114·3	2
$C_6H_6.CuAlCl_4$	2·078	2·143	110·7	3
$TeCl_3.AlCl_4$	2·087	2·142	110·7	4
$SeCl_3.AlCl_4$	2·09	2·137	110·9	5
$Te_4.(AlCl_4)_2$	2·093	2·130	111·1	6
$(CH_3)_7C_6.AlCl_4$	2·105	2·125	109·5	7
$CH_3CO.AlCl_4$	2·120	2·127	110·4	8
$C_6H_6.AgAlCl_4$	2·15	2·13	109·3	9
$SeCl_3.AlCl_4$	2·17	2·13	109·1	5
$(Pd.C_6H_6.AlCl_4)_2$	2·18	2·113	107·4	10
$Hg_3.(AlCl_4)_2$	2·181	2·115	107·4	11
	2·185	2·123	106·4	
$Te_4.(Al_2Cl_7)_2$	2·222	2·103	105·6	6
$(Pd.C_6H_6.Al_2Cl_7)_2$	2·25	2·097	105·7	10
$Te_4.(Al_2Cl_7)_2$	2·262	2·102	104·6	6
$(Pd.C_6H_6.Al_2Cl_7)_2$	2·28	2·097	103·3	10
$AlCl_3(g)$	∞	2·06	90	12

References: (1) McMullan, Prince & Corbett (1971). (2) Cesari, Pedretti, Zazzetta, Lugli & Marconi (1971). (3) Turner & Amma (1966*a*). (4) Krebs, Buss & Altona (1971). (5) Stock-Blaisse & Romers (1971). (6) Couch, Lokken & Corbett (1972). (7) Baenziger & Nelson (1968). (8) Le Carpentier & Weiss (1972). (9) Turner & Amma (1966*b*). (10) Allegra, Tettamanti Casagrande, Immirzi, Porri & Vitulli (1970). (11) Ellison, Levy & Fung (1972). (12) Zasorin & Rambidi (1967).

We first assume that for all points along the correlation curve, $n_1 + 3n_2 = 4$. We then need a relation between bond number and bond angle and we have chosen $n_1 = 9\cos^2\alpha$, $n_2 = \frac{4}{3} - 3\cos^2\alpha$,* where α stands for $\langle\alpha\rangle_{12,13,14}$. This satisfies the desired conditions (1) $n_1 = 1$ for $\alpha = 109{\cdot}47°$; (2) $n_1 = 0$ for $\alpha = 90°$; (3) $d(\delta r_2)/d(\delta\alpha) = 0$ for $\alpha = 90°$. Note, however, that for $\alpha > 131{\cdot}8°$ n_2 becomes zero and hence r_2 becomes infinite. The expected asymptotic behaviour of $\delta r_2 = -c \log(\frac{4}{3} - 3\cos^2\alpha)$ can be discerned in the experimental distribution for $YSnCl_3$ fragments (MBD 1).

* The quadratic dependence of n on $\cos\alpha$ also happens to give better agreement between observed and calculated C—O distances in our study of the nucleophilic addition of amine N to carbonyl than the linear dependence assumed in Bürgi, Dunitz & Shefter (1973).

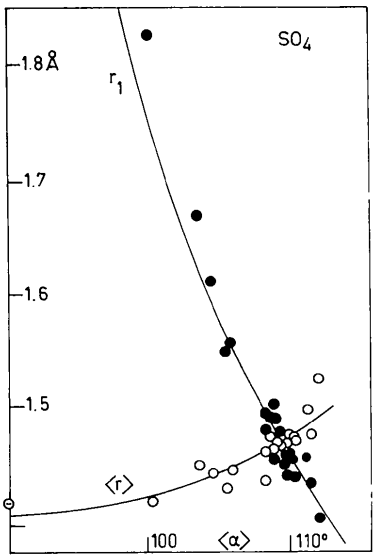

Fig. 8. Distributions of r_1 against $\langle\alpha\rangle_{12,13,14}$ (black circles) and of $\langle r\rangle_{2,3,4}$ against $\langle\alpha\rangle_{12,13,14}$ (white circles) for SO_4 fragments with approximate C_{3v} symmetry. (Not all points in the neighbourhood of $\alpha \sim 109{\cdot}5°$ are shown. The smooth curves are discussed in the text.)

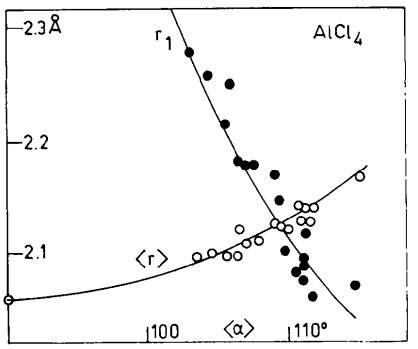

Fig. 9. As Fig. 8, but for $AlCl_4$ fragments (all points shown).

We have determined the numerical constants r_0 and c in the Pauling relation for PO_4, SO_4 and $AlCl_4$ fragments separately by minimizing

$$\sum \{[r_1(\text{obs}) - r_1(\text{calc})]^2 + 3[\langle r\rangle_{2,3,4}(\text{obs}) - \langle r\rangle_{2,3,4}(\text{calc})]^2\}/\sigma^2 \quad (9)$$

where σ is the average e.s.d. quoted for r_i; the factor 3 is introduced because $\langle r\rangle_{2,3,4}$(obs) is the mean of three observations. The r_1 terms for the two planar structures SO_3 and $AlCl_3$ were set equal to zero. The linear least-squares minimization leads to:

$r_0 = 2{\cdot}125$ Å,	$c = 0{\cdot}49$ Å	for $AlCl_4$
1·534	0·47	PO_4
1·472	0·51	SO_4 .

The near equality of c for the three groups conforms with our earlier comment that the sample points, referred to a common origin, appear to be drawn from a single population. A c value of 0·50 Å has been found (MBD 1) to reproduce the main trends in the corresponding distributions for many YMX_3 and non-planar MX_3 (*e.g.* SO_3^{2-}) fragments. It seems remarkable that such a simple model should account quantitatively for bond lengths and angles in a wide variety of molecules. Since the theoretical curves fit the data for quite large deviations from T_d symmetry and even account for the structures of SO_3 and $AlCl_3$, our premise leads us to regard these curves as approximate reaction pathways for ligand dissociation (MBD 1).

7. Effects of crystal environments

So far we have concentrated on the more obvious trends displayed by the experimental distributions but have paid no attention to the deviations of individual sample points from regression lines or correlation curves. Several causes (including experimental errors in the widest sense) can be invoked for these deviations. In the first place, our basic premise does not imply that there should be perfect correlation between the parameters in question. Rather, it suggests that sample points, representing structures in different environments, should have, in the appropriate deformation space, a multivariate distribution whose second moments about the respective means will tend to be small in directions of large increase of potential energy. The position of a particular sample point in the distribution will depend not only on the shape of the energy hypersurface but also on the perturbation produced by the particular environment of the structural fragment in question. This perturbation cannot be expected to act only along the direction of minimum increase of potential energy; it will in general also produce deformations perpendicular to this direction, and indeed, in some cases, these may be the only ones.

Many of the MX_4 fragments considered in this analysis are anionic. For uniformity of description we classify any H atoms that may be attached to an MX_4 fragment as protons, *i.e.* as belonging to the environment of the fragment, and similarly for other covalently bound atoms or groups. It is clear that any large distortion from T_d symmetry can, in principle, be regarded as a response to the interactions between the fragment in question and a particular environment containing cations. We can see that large distortions preserving C_{3v} symmetry should occur for monoprotonated species or for crystal arrangements where a cation is much closer to one vertex of the MX_4 fragment than to the other three. Along the same lines, large distortions preserving C_{2v} symmetry are expected for diprotonated species or for arrangements where cations approach two vertices or where they straddle an edge of the tetrahedron. In § 5 we mentioned that large distortions preserving C_{3v} symmetry could serve to delineate reaction pathways for ligand dissociation, *e.g.* $AlCl_4^- \rightarrow AlCl_3 + Cl^-$, but it would be more correct to explicitly recognize the role of the cation and rewrite the reaction in question as $AlCl_4^- + M^+ \rightarrow AlCl_3 + MCl$; and similarly for the sulphate dissociation.

Although a detailed analysis of every given situation is feasible in principle (McGinnety, 1972) it would be tedious and complicated in practice, especially in view of the heterogeneity of the environments in which our fragments occur.

For all practical purposes, it is virtually impossible to define parameter spaces that encompass the structural parameters of the fragment *and* its environments. We therefore have to restrict ourselves to the changes in the structure of the fragment itself and try to map the deformation path in the corresponding parameter space. However, it is important to recognize that this deformation path is actually obtained by projecting sample points in spaces of higher dimensionality on the subspace of the fragment alone. In this sense, the path may be said to describe the response of the fragment to external forces.

It is an open question how closely this deformation path follows a minimum-energy path in the potential-energy hypersurface of the isolated fragment. We expect a close correspondence between these paths when the energy valley of the isolated fragment has very steep sides, a less close correspondence for relatively shallow valleys and large external perturbations. Too little information is available to draw detailed conclusions.

The only case we discuss here in any detail is that of $LuPO_4$ where the PO_4^{3-} anion has crystallographic D_{2d} symmetry (Lohmüller, Schmidt, Deppisch, Gramlich & Scheringer, 1973). In this situation, there can be no deformation along the $\mathbf{S}_3$, $\mathbf{S}_4$ or $\mathbf{S}_{2b}$ coordinates. From the observed bond length and angles [1·533 Å, 102·5° (twice) and 113·1° (four times)], we obtain $D_1(A_1) \sim 0$,

Table 3. *Structural parameters for* 12 PO_4 *fragments with approximate* C_{2v} *symmetry sharing one or two* O···O *edges with a cation*

Identification numbers are those of Baur's (1974) compilation.

Number	$\langle r\rangle_{3,4}$	α_{34}	α_{34}(corr)	$\langle r\rangle_{1,2}$	α_{12}	α_{12}(corr)
Cation bridging O(1)···O(2) edge						
552	1·470 Å	117·6°	117·1°	1·580 Å	102·3°	101·8°
551	1·481	116·7	118·4	1·592	98·8	100·5
572	1·489	116·6	117·3	1·611	100·9	101·6
554	1·492	116·6	118·0	1·570	99·5	100·9
582	1·509	106·8	110·8	1·577	104·0	108·0
Cation bridging O(3)···O(4) edge						
201	1·518	108·6	111·9	1·534	103·7	107·0
462	1·519	110·6	112·4	1·547	104·7	106·5
414	1·534	109·3	111·3	1·551	105·6	107·6
881	1·534	111·1	110·5	1·538	109·1	108·5
941	1·536	110·0	113·0	1·550	103·0	106·0
Cations bridging both edges						
821	1·502	115·0	114·0	1·590	106·0	105·0
1291	1·533	102·5	109·5	1·533	102·5	109·5

$D_{2a}(E) = -12{\cdot}2°$, the largest $\mathbf{S}_{2a}$ deformation among the 211 PO_4 fragments listed by Baur (1974), and it occurs with the smallest possible value of $|\mathbf{D}_4|$, *i.e.* zero. This structure thus represents a striking exception to the general rule that $\mathbf{D}_4$ angular deformation vectors tend to be larger than those of $\mathbf{D}_2$.

In $LuPO_4$ the phosphate group shares two opposite edges with Lu coordination polyhedra. The large negative $\mathbf{S}_{2a}(E)$ distortion corresponds to a compression of two opposite angles. By analogy with $LuPO_4$ we might expect other bridged PO_4 fragments to show appreciable deformations along $\mathbf{S}_{2a}(E)$. We have selected 11 such fragments with approximate C_{2v} symmetry and sharing one or two edges with cations lying close to the approximate twofold axis. Table 3 reveals that contributions from $\mathbf{S}_{2a}(E)$ deformations to $\delta\alpha_{ij}$ [see (3)] amount to as much as 7° in some of these fragments. The extra scatter produced by these contributions will tend to obscure some of the correlations that would be present if the total deformation were exclusively along $\mathbf{S}_{3a}$ and $\mathbf{S}_{4a}$. Fig. 10(*a*) shows the distribution of $\langle r\rangle_{i,j}$ against included angle α_{ij} for the 12 PO_4 fragments with shared edges. Fig. 10(*b*) is the distribution for the same 12 fragments with the $D_{2a}(E)$ component removed, *i.e.* $\langle r\rangle_{i,j} = (D_1 \pm D_{3a})/2$ and $\alpha_{ij}(\text{corr}) = 109{\cdot}47° \mp D_{4a}/\sqrt{2}$ [compare (3)]. The scatter at small α_{ij} has obviously been reduced by this procedure. This result shows once again that any correlation that may be present is to be seen more clearly in terms of symmetry coordinates than in terms of internals. It also indicates how the effects of special environments (here, shared edges) can be accounted for, once they are recognized as such.

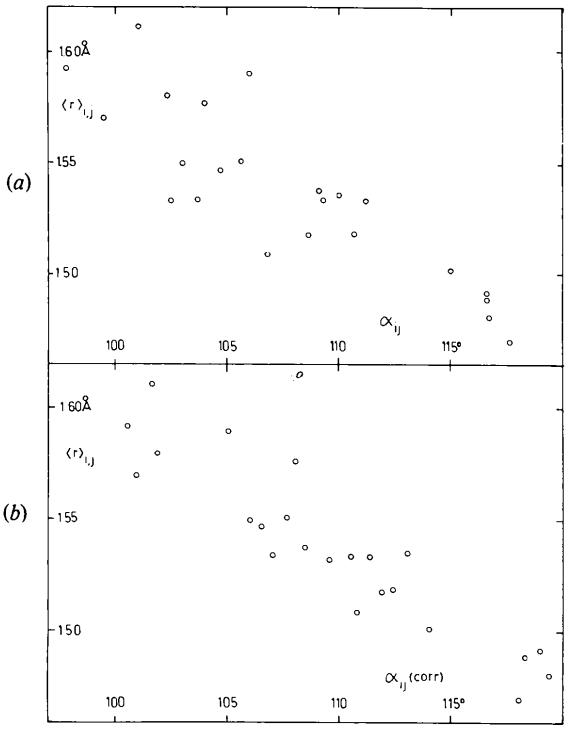

Fig. 10. (*a*) Distribution of $\langle r\rangle_{i,j}$ against α_{ij} for 12 PO_4 fragments (Table 3) with shared edges. (*b*) Same data with $D_{2a}(E)$ contribution to α_{ij} subtracted out [see (3)].

Of course, every environment is a special environment. For our approach to be workable, it suffices to assume that the net effect of the various crystalline

environments encountered by our fragment is to produce a representative distribution of sample points over the low-energy regions of the appropriate hypersurface. Whether this assumption is valid or not is another matter. One could imagine, for instance, that Baur's (1974) list of 211 PO_4 fragments contained not one but a hundred examples with D_{2d} symmetry, in which case we would have come to very different conclusions about the relative ease of deformation along different symmetry coordinates. In the last resort we have no option but to trust that the output from our crystallographic colleagues represents a more or less random selection of realizable structures.

One of us (PM-R) is indebted to the Ciba–Geigy Fellowship Trust for the award of a Senior European Research Fellowship.

References

ALLEGRA, G., TETTAMANTI CASAGRANDE, G., IMMIRZI, A., PORRI, L. & VITULLI, G. (1970). *J. Am. Chem. Soc.* **92**, 289–293.

BAENZIGER, N. C. & NELSON, A. D. (1968). *J. Am. Chem. Soc.* **90**, 6602–6607.

BARTELL, L. S., SU, L. S. & YOW, H. (1970). *Inorg. Chem.* **9**, 1903–1912.

BAUR, W. H. (1970). *Trans. Am. Crystallogr. Assoc.* **6**, 129–155.

BAUR, W. H. (1974). *Acta Cryst.* B**30**, 1195–1215.

BERGIN, R. & CARLSTRÖM, D. (1971). *Acta Cryst.* B**27**, 2146–2152.

BROWN, G. M. & CHIDAMBARAM, R. (1969). *Acta Cryst.* B**25**, 676–687.

BROWN, I. D. (1969). *Bond Index to the Determinations of Inorganic Crystal Structures.* Institute for Materials Research, McMaster Univ., Hamilton, Ontario, Canada.

BROWN, I. D. & SHANNON, R. D. (1973). *Acta Cryst.* A**29**, 266–282.

BÜRGI, H. B. (1973). *Inorg. Chem.* **12**, 2321–2326.

BÜRGI, H. B., DUNITZ, J. D. & SHEFTER, E. (1973). *J. Am. Chem. Soc.* **95**, 5065–5067.

BÜRGI, H. B., DUNITZ, J. D. & SHEFTER, E. (1974). *Acta Cryst.* B**30**, 1517–1527.

CESARI, M., PEDRETTI, U., ZAZZETTA, A., LUGLI, G. & MARCONI, W. (1971). *Inorg. Chim. Acta*, **5**, 439–444.

CLARK, A. H. & BEAGLEY, B. (1971). *Trans. Faraday Soc.* **67**, 2216–2224.

COUCH, T. W., LOKKEN, D. A. & CORBETT, J. D. (1972). *Inorg. Chem.* **11**, 357–362.

DOLLASE, W. A. (1969). *Acta Cryst.* B**25**, 2298–2302.

DONALDSON, J. D. & PUXLEY, D. C. (1972). *Acta Cryst.* B**28**, 864–867.

ELLISON, R. D., LEVY, H. A. & FUNG, F. W. (1972). *Inorg. Chem.* **11**, 833–836.

FRIES, D. C. & SUNDARALINGAM, M. (1971). *Acta Cryst.* B**27**, 401–410.

HOLMES, R. R. & DEITERS, J. A. (1977). *J. Am. Chem. Soc.* **99**, 3318–3326.

JÖNSSON, P. G. & HAMILTON, W. C. (1970). *Acta Cryst.* B**26**, 536–546.

KAY, M. I. & CROMER, D. T. (1970). *Acta Cryst.* B**26**, 1349–1355.

KJÄLLMAN, T. & OLOVSSON, I. (1972). *Acta Cryst.* B**28**, 1692–1697.

KREBS, B., BUSS, B. & ALTONA, D. (1971). *Z. Anorg. Allg. Chem.* **386**, 257–269.

LAGER, G. A. & GIBBS, G. V. (1973). *Am. Mineral.* **58**, 756–764.

LE CARPENTIER, J.-M. & WEISS, R. (1972). *Acta Cryst.* B**28**, 1421–1429.

LOHMÜLLER, G., SCHMIDT, G., DEPPISCH, B., GRAMLICH, V. & SCHERINGER, C. (1973). *Acta Cryst.* B**29**, 141–142.

MCDONALD, W. S. & CRUICKSHANK, D. W. J. (1967). *Acta Cryst.* **22**, 37–43.

MCGINNETY, J. A. (1972). *Acta Cryst.* B**28**, 2845–2852.

MCMULLAN, R. K., PRINCE, D. J. & CORBETT, J. D. (1971). *Inorg. Chem.* **10**, 1749–1753.

MORIMOTO, C. N. & LINGAFELTER, E. C. (1970). *Acta Cryst.* B**26**, 335–341.

MOROSIN, B. & HOWATSON, J. (1970). *Acta Cryst.* B**26**, 2062–2072.

MUETTERTIES, E. L. & GUGGENBERGER, L. J. (1974). *J. Am. Chem. Soc.* **96**, 1748–1756.

MURRAY-RUST, P., BÜRGI, H. B. & DUNITZ, J. D. (1975). *J. Am. Chem. Soc.* **97**, 595–596.

MURRAY-RUST, P., BÜRGI, H. B. & DUNITZ, J. D. (1978). *Acta Cryst.* B**34**, 1787–1793.

NELMES, R. J. (1971). *Acta Cryst.* B**27**, 272–281.

PALMER, K. J., WONG, R. Y. & LEE, K. S. (1972). *Acta Cryst.* B**28**, 236–241.

PAULING, L. (1947). *J. Am. Chem. Soc.* **69**, 542–553.

PRUSINER, P. & SUNDARALINGAM, M. (1972). *Acta Cryst.* B**28**, 2142–2148.

SCHAEFFER, W. P. & LIGHTY, R. A. (1972). *Acta Cryst.* B**28**, 1777–1784.

SIKKA, S. K. & CHIDAMBARAM, R. (1969). *Acta Cryst.* B**25**, 310–315.

STOCK-BLAISSE, B. A. & ROMERS, C. (1971). *Acta Cryst.* B**27**, 386–392.

SUBRAMANIAN, E. & MARSH, R. E. (1971). *Acta Cryst.* B**27**, 753–759.

THEWALT, U. (1971). *Acta Cryst.* B**27**, 1744–1752.

TURNER, R. W. & AMMA, E. L. (1966*a*). *J. Am. Chem. Soc.* **88**, 1877–1882.

TURNER, R. W. & AMMA, E. L. (1966*b*) *J. Am. Chem. Soc.* **88**, 3243–3247.

VAN DER HELM, D. & NICHOLAS, H. B. (1970). *Acta Cryst.* B**26**, 1858–1866.

VRIES, R. DE & MIJLHOFF, F. C. (1969). *Acta Cryst.* B**25**, 1696–1699.

ZASORIN, E. Z. & RAMBIDI, N. G. (1967). *Zh. Strukt. Khim.* **8**, 391–397.